Autocorrelated Differential Algorithm for Real-Time Seismocardiography Analysis

Yannick D'Mello, *Member, IEEE*, James Skoric, Shicheng Xu, Megan Akhras, Philip J. R. Roche, Michel A. Lortie, Stéphane Gagnon, and David V. Plant, *Fellow, IEEE*

***Abstract*— We present a novel seismocardiography (SCG)-based approach for real-time cardio-respiratory activity measurement called the Autocorrelated Differential Algorithm (ADA). Measurements were performed on ten male subjects in the supine position for three 7-minute-long sets each, corresponding to 14,619 heartbeats. The ADA utilized temporal variations, windowing, and autocorrelation to produce physiological measurements corresponding to heart rate (HR), and left ventricular ejection time, and estimations of respiration rate, volume, and phase. The versatility of the ADA was investigated in two contexts: physical exertion and heart rate variability. The accuracy of HR measurements at a sampling frequency of 200 Hz resulted in a correlation coefficient (r^2) of 0.9808 when compared with a manual annotation of all datasets. Its reproducibility was tested on externally obtained SCG and electrocardiography datasets, which produced an r^2 of 0.8224. The accuracy and computational time were also characterized by different sampling frequencies to quantify performance. The recommended sampling frequency is 200 Hz corresponding to a computation time of 0.05 s per instantaneous measurement using a standard desktop computer. The ADA delivered real-time SCG measurements with a refresh rate that was dependent on the computational time per measurement, which could be decreased by lowering the sampling frequency. The presented algorithm offers a novel tool toward real-time physiological monitoring in clinical and everyday scenarios.**

***Index Terms*— Seismocardiography, autocorrelation, heart rate, respiration rate, cardiac time intervals, real-time, digital signal processing.**

I. Introduction

THE continuous and portable monitoring of cardiac and respiratory activity has attracted significant interest among the healthcare community in recent years due to the increasing prevalence of cardiac and respiratory ailments. Cardiovascular diseases are one of the highest contributing factors to global mortality rates [1]. Additionally, increased pollution levels in major cities have prompted governments to fund research into the investigation of respiratory ailments [2]. Accurate diagnosis is instrumental in the detection, prevention, and cure of such issues as the symptoms are not always obvious. This demand highlights the need for portable devices capable of measuring cardio-respiratory activity (CRA) as and when required. Knowledge of a subject's physiological activity prior to, during, and after events such as stroke, cardiac arrest, or breathlessness can enable a deeper insight into the causes and symptoms of these issues. The data collected from the continuous, portable monitoring of CRA will therefore enable a deeper, long-term evaluation of the relationship between measurements and physiological wellbeing, improve the efficiency of medical treatment, and contribute to the development of prediction algorithms for health state trajectories.

A number of methods have been established that deliver measurements of cardiac activity. Photoplethysmography is a portable measure of peripheral oxygen saturation (SpO_2) in the blood from which heart rate may be derived, but is sensitive to variations in ambient light and skin contact [3]. Other methods exist such as ballistocardiography (BCG), which measures full-body microaccelerations and requires the use of a weighing scale or bed [4]; sphygmomanometry uses bulky instrumentation to produce accurate albeit discretized measurements [5]; and phonocardiography, a measure of heart sounds, lacks the ability to pinpoint the timing corresponding to valvular moments [6]. Alternatively, the movements caused by CRA within the diaphragm manifest as vibrations on the surface of the chest, which can be non-invasively detected by miniaturized inertial sensors based on micro-electro-mechanical systems (MEMS) technology. The method of measuring myocardial vibrations through acceleration at the sternum is termed seismocardiography (SCG) [7]–[9]. The extraction of respiration rate from the acceleration signal produced by the SCG waveform [10]–[13] enables an analysis of the coupling between respiration and myocardial activity, which is a contributing factor to heart rate variability (HRV) [14]–[17]. The direct causal relationship between CRA and SCG enables an accurate interpretation of cardiac mechanics and therefore muscle activity, especially in high-risk subjects [18] or those with congenital heart defects. The ability to measure cardiac mechanics overcomes a limitation of electrocardiography (ECG), which is confined to measuring electrical activity of the heart but not the consequent contractions of the muscle [19] that are responsible for circulation. Outside of the clinic, SCG offers a promising approach that could provide continuous health monitoring at home and in

Manuscript received January 15, 2019; revised February 15, 2019; accepted February 22, 2019. Date of publication March 7, 2019; date of current version June 4, 2019. This work was supported in part by the National Sciences and Engineering Research Council (NSERC) of Canada, in part by the MacDonald, Dettwiler and Associates Corporation, and in part by McGill University. The associate editor coordinating the review of this paper and approving it for publication was Prof. Aime Lay-Ekuakille. *(Corresponding author: Yannick D'mello.)*

Y. D'Mello, J. Skoric, S. Xu, M. Akhras, P. J. R. Roche, and D. Plant are with the Department of Electrical and Computer Engineering, McGill University, Montreal, QC H3A 2T5, Canada (e-mail: yannick.dmello@mail.mcgill.ca).

M. A. Lortie and S. Gagnon are with the MacDonald, Dettwiler and Associates Corporation, Ottawa, ON K2K 1Y5, Canada.

Digital Object Identifier 10.1109/JSEN.2019.2903449

mobile circumstances due to its unobtrusive and continuous monitoring capabilities [20]–[22].

The shape and timing of fiducial points in the seismocardiogram has the potential to detect cardiac conditions [23] including ischemia [24], [25], and hemorrhage [26], and also enable hemodynamic assessments. However, a significant difficulty with CRA measurements is inter-subject variations, which necessitates robust and adaptable digital signal processing (DSP) algorithms [27]. The current state of the art regarding accuracy in SCG-DSP includes algorithms that either perform an analysis of the signal offline due to high computational requirements [28]–[30], that require synchronized measurements with ECG [21], [31], or that implement pre-training for calibration to the user [32], [33]. Caveats such as these preclude the implementation of SCG in real-time, portable cardiac analysis. Still, there exist ECG-less algorithms [27], [34], [35] that deliver high accuracy, real-time heart rate detection by using techniques such as adaptive thresholding, envelope or spectral-based analyses, and autocorrelation. However, envelope or spectral methods are limited in their classification of intra-beat cardiac time intervals (CTIs) and SCG morphology within individual cardiac cycles. Additionally, the estimation of fiducial points using fixed thresholds is limited by the dependence on signal quality. The most common drawback of autocorrelation techniques for SCG analysis is the damping of HRV due to the inherent averaging of many beats, or poor correlation between consecutive cardiac cycles due to HRV itself. This negates the value of cardiac monitoring in measuring palpitations, attacks, or arrhythmia, which are vital to the early detection of CVDs [36]–[38]. The accuracy of most SCG-DSP algorithms is dependent on signal quality and minimal heart rate variability between SCG cycles. The detection of CRA taking into account variability, motion artifact and noise suppression are necessary objectives for the realization of a cost-effective system.

In this paper, we present an algorithm that provides a real-time evaluation of cardiac activity based on the autocorrelation technique, and consequently extract respiration metrics. Signal amplification relied on the waveform morphology, which will be described in Section II.A followed by the protocol used for SCG signal acquisition in Section II.B and a description of the autocorrelation approach and its utility in Section II.C. Regarding the algorithm, variable windowing of the signal facilitated instantaneous detection and reduced the smoothing effect inherent to autocorrelation techniques as will be explained in Section III.A. The autocorrelation was performed on a filtered SCG, after the extraction of respiratory information as detailed in Section III.B. Variations in the filtered signal morphology were accounted for by exploiting the consistency in the shape of the S1 feature between consecutive beats in any SCG signal as explained in Section III.C. The versatility of the approach was evaluated by including intra-subject dynamic variations for resting heart rates, as well as varying amplitude and frequency SCG signals obtained from physically exerted subjects in Section IV.A. The accuracy was measured in Section IV.B by evaluating its correlation with a manual annotation of all SCG datasets and with an external database containing both SCG and ECG signals. The analysis was further extended in Section V, to an investigation of CTIs as well as performance characterization for accuracy and computational time. The paper is concluded in Section VI along with final remarks.

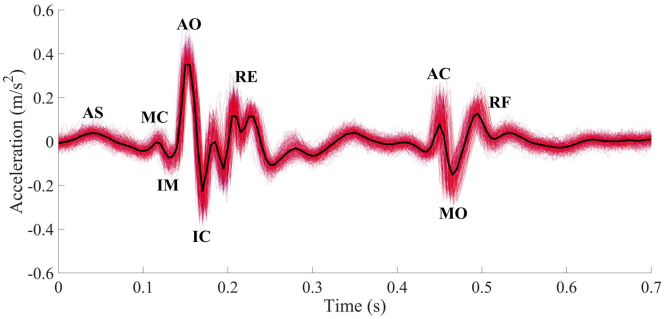

Fig. 1. Time-averaged SCG waveform (black) of 300 consecutive cardiac cycles (red) from a supine subject in a relaxed state. The annotations indicate inflection points in the morphology of the waveform corresponding to specific events in a regular cardiac cycle [19].

II. Methods

A. Seismocardiogram Morphology

The SCG waveform for each cardiac cycle consists of certain fiducial points that correspond to specific events in the cardiac cycle. These events [19] are labeled in Fig. 1 for an experimentally measured SCG pattern obtained by averaging 300 consecutive cardiac cycles from a subject at rest. The inflection points indicate the mitral valve closure (MC), isovolumetric moment (IM), the aortic opening (AO), isotonic contraction (IC), and rapid ejection (RE) of blood to the body, within the systolic phase of the cardiac cycle. The diastolic phase starts with the aortic closure (AC) for refilling of the left ventricle, and is followed by the mitral opening (MO) and the rapid flow (RF) of blood refilling the heart. The accurate detection of these events is necessary for the calculation of CTIs [39] such as the pre-ejection period [40], systolic period (QS2), left ventricular ejection time (LVET) [41], and diastolic period [42] which quantify myocardial performance and functionality [43], [44].

The primary cardiac sound S1 originates in the W-complex described by the MC-IM-AO-IC-RE fiducial points. The middle peak-valley-peak pattern formed by the AO-IC-RE events is of particular interest as it is a prominent feature of any SCG waveform, and is used in this algorithm as a reference point to distinguish cardiac cycles. The AC-MO region causes the second sound S2, which if sufficiently strong, may interfere with S1 detection in algorithms that rely on envelopes or AO peak thresholding for heart rate evaluation. With issues such as respiratory sinus arrhythmia [45], the amplitude of S2 may be larger than S1, which can reduce the accuracy of more advanced algorithms [34]. We therefore took into account the oscillation amplitude and shape of the S1 feature during detection.

B. Protocol for Data Acquisition

The study was conducted on 10 male subjects between 20 and 30 years old. Similar to other SCG-based studies, only

subjects with no prior knowledge of heart conditions were considered. All data was collected with approval from the Research Ethics Board at McGill University. Each subject was measured in the supine position during three data collection sets, each with a duration of 7 minutes. The first two sets were conducted with the subject relaxed, after which, the subject was made to perform a Mountain Climber exercise to induce physical exertion [46]. The third set was collected immediately after the exercise to obtain information relating to the trajectory of the subject's physiological recovery pattern.

SCG data was collected by strapping an InvenSense MPU-9250 inertial measurement unit (IMU) on the xiphoid process of the sternum with the accelerometer X, Y, and Z axes oriented right along the sinistro-dexter, upward along the inferior-superior, and outward along the dorsoventral axes, respectively. The MPU-9250 was sampled at a frequency of 250 Hz with the acceleration set to its lowest resolution of ± 2 g, where 1 g equals 9.8 m/s^2. It was interfaced through an I2C link to an Arduino Leonardo microcontroller. Data from the Arduino was sent to a computer serially and processed in MATLAB.

The medical device used as a reference was an Omron S10 cuff sphygmomanometer strapped to the upper left arm. For each cuff measurement, the timing of occurrence of two distinct events were logged: (i) the beginning of the cuff deflation which marked the start of the measurement process, and (ii) the time at which the cuff deflated completely marking the finished process. The cuff automatically performed three consecutive, independent heart rate measurements spaced 60 seconds apart in each set. The results were used as a baseline verification of HR measurements, but considering the large window of uncertainty regarding the timing of measurement, and the low frequency of measurements, they were not used to quantify the real-time accuracy. In this context, the experimental data obtained from the cuff was manually synchronized with the SCG monitor. This was justified because the human error introduced via manual logging (less than 1s) was negligible as compared to the temporal uncertainty of the cuff measurements. As an additional layer of verification, every SCG dataset was manually annotated at the AO points to provide a reference for the detection of AO points using the code.

C. Utilization of Autocorrelation

The choice of autocorrelation as the basis of the Auto-correlated Differential Algorithm (ADA) was motivated by two factors: the quasi-periodicity of cardiac cycles, and the consistency in the shape of the S1 feature for a given heart despite arrhythmia or variability.

Previous techniques employing template-based cross-correlation to detect averaged heart rate in BCG [47] and SCG [48] signals have demonstrated an ability to accurately measure heart rate when subjected to only small variations in inter-beat intervals. However, significant HRV is common in healthy hearts and accurate HRV analysis is necessary for the interpretation of CTIs [49] as it offers insight into the interplay between the sympathetic and parasympathetic nervous system.

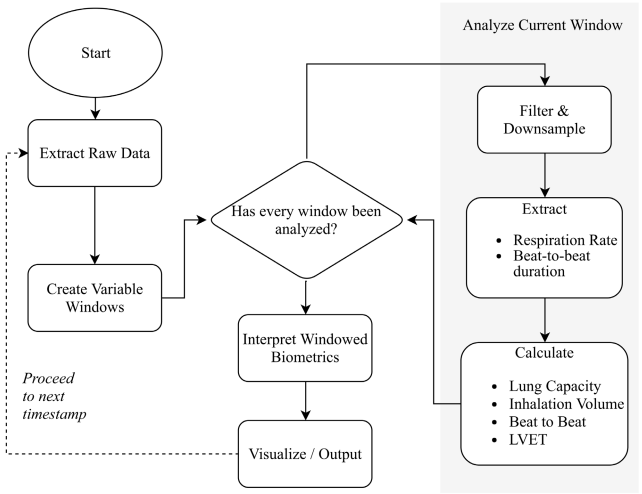

Fig. 2. Process flowchart of the Autocorrelated Differential Algorithm. The raw accelerometer signal was first split into multiple windows of increasing size. Each window was analyzed assuming no variation within the window. The data was down-sampled and filtered for each measurement, and subsequently analyzed. The resulting measurements were delivered to the algorithm for further processing and visualization.

A common limitation in autocorrelation-based algorithms is therefore their ability to measure HRV and more severely, issues such as murmurs or atrial fibrillation [50]. We overcome this limitation by windowing the autocorrelation function using increasing window sizes. The autocorrelation was performed on a filtered SCG with respiratory oscillations subtracted from the raw signal. This extraction did not take into account the modulation of cardiac activity by respiration [51]. Such variation in cardiac activity typically limits the scope of autocorrelation algorithms, along with other variations caused by HRV, sensor position and signal quality, interpersonal variations in SCG morphology, exertion levels, etc. These variations were considered by exploiting the consistency in the shape of the S1 feature between consecutive beats in any SCG signal as will be explained in the next section.

III. Auto-Correlated Differential Algorithm

In keeping with the functionality of a heart-rate monitor, the ADA was designed to update its delivery of physiological measurement calculations with a refresh rate of one second. This implied that the ADA could only be considered a real-time system when run on a processor with a computing power capable of processing data using the algorithm, in under a second. The implicit speed requirement was realized using any commercially available processor (as explained in Section V-A and ran at a computational time of under 0.05 seconds per measurement, corresponding to one second of data collection. The process flow of the algorithm is shown in Fig. 2, where signal processing was performed on a four-column matrix consisting of the three co-ordinate axes, and a fourth axis comprising of the vector magnitude of the three axes.

A. Windowing

Raw, accelerometer data was acquired from a subject using the protocol described in Section I.B. The time signatures of

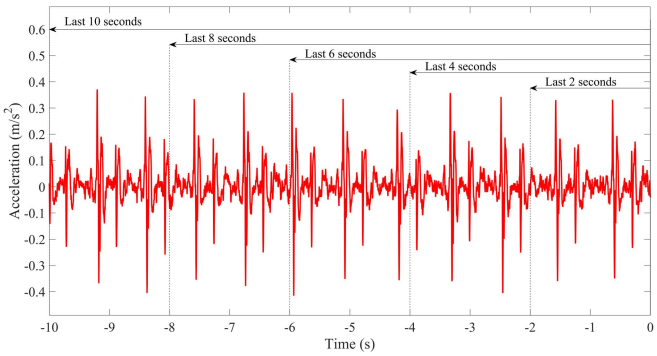

Fig. 3. Windowing of the accelerometer data. Each window starts at time $t = 0$ s or "now" and extends backwards for a specific number of seconds. Cardiac activity was analyzed in the smaller windows and respiratory activity analysis was prioritized in the larger windows.

the signal were first down-sampled to a frequency of 200 Hz using a pchip interpolation. This frequency was found to result in minimal loss in accuracy while maintaining a computational time of less than 1 second, per second of measurement. The choice of sampling frequency retained any significant SCG features that lied within the spectrum up to 100 Hz as determined by the Nyquist theorem, considering most of the SCG spectrum is speculated to exist until approximately 20 Hz [42]. The pchip interpolation technique accounted for any discretization errors caused by inconsistent lags in the data transfer between the accelerometer and the computer. The data stream at each time instance was then partitioned into varying window sizes consisting of 2 to 10 s periods as depicted in Fig. 3, with each window ending at $t = 0$s or the timestamp corresponding to 'now'. The maximum window size of 10 s was stipulated by the maximum allowable delay before a medical device would be required to issue a warning if abnormal CRA was detected [52].

The implementation of this windowing approach was designed to overcome the limitation of autocorrelation algorithms to maintain accuracy over varying rates of cardiac and respiratory activity. Note that the periodicity of a cardiac cycle with respect to a measurement was assumed constant within any given window. Analysis was then performed on each windowed segment separately for consistency and redundancy. The results from all windows were compared with each other using suitable decision-making algorithms, which determined the appropriate value to be assigned to each physiological measurement. This process was repeated for each new second of data that the system received.

B. Respiratory Activity: Frequency Domain Extraction

The higher amplitude respiratory component was filtered from the accelerometer signal for SCG analysis. The extraction process enabled estimations of respiratory activity from the signal corresponding to respiration rate, inhalation volume, lung capacity, and respiration phase as follows:

1) Respiration Rate: Expansion of the diaphragm during respiration causes corresponding oscillations in acceleration at the sternum. However, as the lungs are located above the xiphoid process and therefore the placement of the IMU, the accelerometer did not move directly outward along the dorsoventral axis – its Z axis. Irrespective of body positioning, the low frequency (typically sub-Hz) acceleration-based oscillations due to respiration were manifested as chest movements in sometimes the X, Y, and Z axes. Hence, the FFTs from all three axes within a specific window were simultaneously considered, assuming a constant respiration rate within the window.

The spectra were first passed through a brick-wall filter with a lower limit of 2.4 breaths/minute. No upper limit was specified in order to account for hyperventilation and coughing. For reference, respiratory monitors are advised to provide a warning within 10 seconds if the rate exceeds 30 breaths/minute [53]. The filter eliminated the lower frequency components related to orientation while retaining any cases of holding ones breath, and eliminated the upper frequency components related to motion artifact while retaining any signs of hyperventilation. The peak frequency of each of the three measured spectra offered an indication of the respiration rate but typically, the peak frequency from each of the three measurement axes was different. The correct peak within each spectrum was therefore chosen through a process of elimination. First, a normalized, weighted mean of all four (X, Y, Z, and magnitude) peak frequencies was calculated by using their corresponding amplitudes as weights. The furthest value from the weighted mean frequency was then eliminated. In the case of two equidistant options from the weighted mean, the value corresponding to a lower amplitude was eliminated. In this way, the respiration rate was calculated as the best option among the frequency spectra, taking into account other amplitudes and axes. Due to the maximum window size set at 10 s, the resolution at the lower end of the frequency spectrum was heavily discretized causing the respiration rate measurement to appear quantized, especially for lower rates when the subject was relaxed.

2) Inhalation Volume: A comprehensive insight into respiratory activity and its effect on the body requires knowledge of the instantaneous inhalation volume, as well as the overall capacity of the lungs for calibration. The signal was parsed to quantify the volume of air that had been inhaled into the lungs until 'now', that is, since the most recently acquired acceleration value from the sensor as it correlated to the current, instantaneous, inhalation volume. In order to accurately determine this value, the signal was segmented into individual respiratory cycles using the previously calculated respiration rate. The most recent cycle was then fitted to a sinusoid with a periodicity similar to the respiration rate. Fig. 4 below shows an 8 s long window with the most recent respiration cycle highlighted, and fitted to a sinusoid. The most recently acquired acceleration value was compared with the amplitude and offset of the sinusoid, and subtracted from the most recent, lowest exhalation point to provide a qualitative estimate of how much air had been inhaled relative to empty lungs. Note that the quantification of volume was limited by unknown factors such as the lung size (estimated from the subject's height), low frequency motion artifacts, and accelerometer drift. Hence, the measured inhalation volume was a relative and not an absolute value. The oscillation

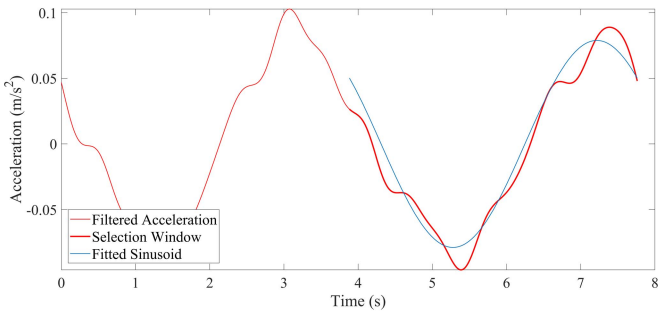

Fig. 4. Acceleration at the diaphragm (red) caused by the respiratory cycle within an ~8 s window. The most recent breath (bold red) was fitted to a sinusoid (blue). The amplitude of the fitted sinusoid offers insight into the smoothed inhalation volume. Its phase or angle indicates that the status of respiration is at the inhalation peak.

amplitude of the fitted sinusoid (corresponding to inhalation volume) was calibrated as a fraction of the lung capacity to quantify the volume of air inhaled or exhaled.

3) Lung Capacity: The maximum capacity of the lungs of a given subject is technically almost constant, but that value cannot be a priori determined without a knowledge of the subject's physical dimensions [54], or preliminary deep breaths for baseline calibration. Hence, lung capacity dynamically evolved with new incoming data. The maximum amplitude of all low-frequency components of respiration, corresponding to the largest breath, provided an indication of the maximum volume of air that had been inhaled in the given window. However, this factor could have been affected by a small window size, irregular breathing, heaving, or movement. Hence, the overall capacity of the lungs was estimated as the mean of the Hilbert envelope [34] of the respiratory cycle, and the amplitude of largest breath. The power spectral density was not used for this calculation since the resolution of the spectrum at low frequencies was significantly low, and since it did not enable a quantification of the capacity of the lungs from chest displacement. The values from multiple windows were aggregated using a weighted mean, with preference given to larger window sizes since normal breathing patterns occurred over multiple seconds.

4) Respiration Phase (Inhalation Vs Exhalation): The phase of inhalation was predicted by using the combination of an instantaneous phase evaluation from the Hilbert transform of the lower frequency components, and by correlating the phase of inhalation to the phase of the peak frequency component of the respiration spectrum. The angle of the fitted sinusoid in Fig. 4 offered insight into the respiratory phase of the subject, namely whether the subject was currently exhaling or inhaling (and its extent). This was extrapolated to offer a prediction as to whether the subject would exhale or inhale next. The inhalation phase was calculated by extracting the phase of the sinusoid corresponding to the current respiration cycle, and verifying it with the instantaneous Hilbert phase. In cases where the phases were in disagreement, the latter half of the respiratory cycle was fitted to a 2nd order polynomial, and the curvature was used to determine the respiratory phase. Note that whilst fitting contributed to robustness by smoothing any irregular peaks, fitting also introduced an accuracy trade-off because this process induced rounding errors of approximately a few milliseconds in cases where one of the double peaks was in fact, the correct peak.

The extraction of phase provided an estimation of the respiratory state of the subject. The quantification of this phase via sinusoid fitting enabled a prediction of the next point in the cycle, which offered insight as to whether the subject would be inhaling or exhaling. Since heart rate is modulated by respiration [51], this information would be useful for motion artifact cancellation and filtering implicit in future iterations of the ADA, as well as more accurate measurements of cardiac activity.

C. Cardiac Activity: Windowed Autocorrelation

Cardiac activity was obtained by amplifying specific features in the SCG corresponding to events at the AO and AC points, and performing an autocorrelation to quantify the periodicity of each feature for a specific window. Analysis of SCG morphology was demonstrated by extracting the left ventricular ejection time (LVET), which is a prominent indication of the systolic time interval [55].

1) Heart Rate: The acceleration signal was passed through a high pass brick-wall filter to eliminate frequencies lower than 0.4 Hz (or 24 bpm), which are typically associated with respiratory activity or changes in orientation. In order to amplify the AO-IC feature, an algorithm called VarWin (variation in window) was created. For each timestamp in the waveform, the function computed the maximum variation between the acceleration at that timestamp $s\,(t)$, and all values within a specific range. The range was pinned to the maximum duration of a heart sound i.e., 0.25 s.

$$f\,(t) = \max\left(s\,(\mathrm{t}) - s\,(t_v)\right), t_v \in [t \pm 0.25s] \tag{1}$$

Thus, significant variations in the SCG between successive inflection points appeared as spikes in the VarWin output as shown in Fig. 5, with the peaks matching the amplitude of oscillation at the areas of strongest variation. This is the 'Differential' aspect of the ADA. The temporal length of the AO-IC feature was shorter than this time window, and furthermore, the temporal range was purposely enlarged so as to spread out or smear the feature for easier detection via autocorrelation. The function hence produced a representation of the SCG waveform, as the output directly related to the shape of the original SCG, but did not completely retain every feature. This was due to the effective 'smearing' of the signal over the specified range, while emphasizing any variations in the signal. The process is therefore not completely reversible. The resultant waveform was a representation of the variations in the SCG using a sliding window. VarWin significantly improved peak detection. It desensitized the ADA to AO amplitude variability and instead focused on the consistent AO-IC variations. 'Smearing' further increased inter-beat correlation and reduced the interference from AC-MO variations.

The waveform was autocorrelated to identify periodicity in the signal by comparing it with a time-delayed copy of itself,

$$A_s\,(\tau) \rightarrow A_f\,(\tau) = \int_{-\infty}^{\infty} f^*\,(t)\, f\,(\tau + t)\, dt \tag{2}$$

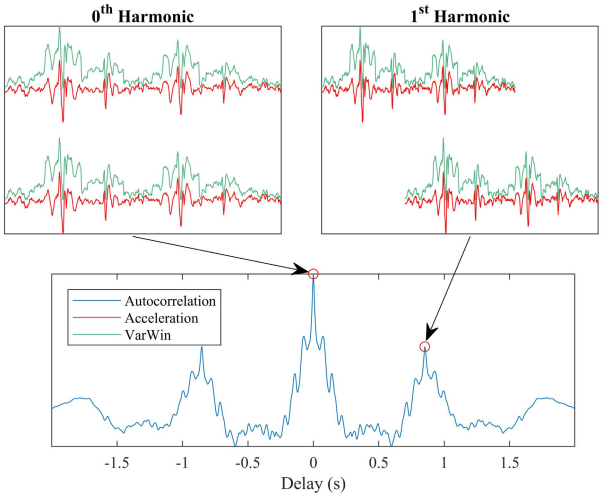

Fig. 5. Visual representation of the SCG (red), VarWin function (green), and an autocorrelation of the VarWin output (blue). The delay between the right and middle peaks is the duration between beats.

Here τ is the delay and t is the timestamp of the signal. The autocorrelation $A_f(\tau)$ waveform generated a series of peaks whenever strong periodic features (AO-IC drops) aligned, as can be seen in Fig. 5. The fundamental harmonic was identified as the strongest peak with an amplitude greater than 15% of the 0^{th} harmonic. Thresholding was necessary to eliminate correlations with AC-MO peaks or noise, whereas we implemented relative thresholding to ensure that a weak signal was still correctly identified. Factors such as HRV, heart efficiency fluctuations, and variations between beats caused additional distortion within the harmonics. The detected fundamental harmonic peak of $A_f(x)$ was therefore fitted with a second order polynomial to smooth discontinuities,

$$A_f\left(x \to \tau; x \in \left[\frac{\tau}{2}, \frac{3\tau}{2}\right]\right) = p(x) = ax^2 + bx + c, a < 0 \tag{3}$$

The delay between the apex of the polynomial and the 0^{th} harmonic was calculated as the inter-beat interval corresponding to the average duration of a cardiac cycle within the given window. This calculation was based on the periodicity of the SCG within 2 to 5 cardiac cycles, and the predictability of the waveform in retaining key SCG features. The instantaneous beat-to-beat interval (BTB) was calculated as the inter-beat interval from the smallest possible window.

The periodicity of SCG is a useful tool to help evaluate the instantaneous BTB, but does not take into account HRV in a healthy heart, which introduces significant fluctuations in real-time heart rate (HR) measurements as shown in Fig. 6. Moreover, all cardiac time intervals are frequency modulated by respiration and nerve activity [14]–[17], [51]. In a general medical examination, HRV is typically factored out by counting the number of beats over one minute. However, the advantage of real-time monitoring would be lost if the biometric signal was smoothed over an entire minute of data acquisition. This is validated by the recovery profile in Fig. 8.b that showed a significant decline in HR during recovery from physical exertion within the first minute. On the other hand, a relatively stable heart rate measurement has higher readability when delivered on a per second basis in a real-time advisory situation as assumed by the ADA design. In order to retain HRV and still smooth the HR to be relatively stable in real-time, the ADA incorporated a windowing function that calculated a normalized, weighted mean of HR from multiple window sizes over the most recent five seconds. Since the smaller windows contained less cardiac cycles, they had a stronger correspondence to the instantaneous HR. Therefore, small windows were given preference in the weighted mean calculation, with the weight being determined by the duration of the window as follows,

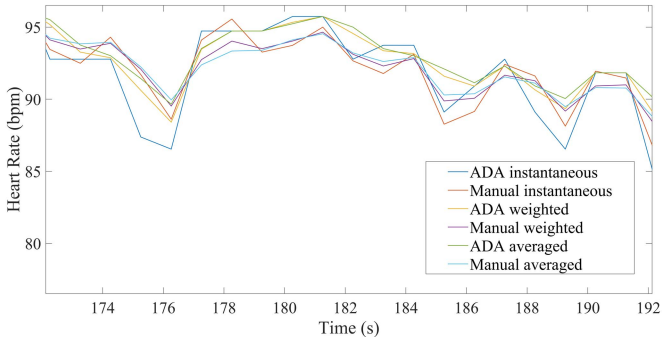

Fig. 6. HR calculated per second from SCG using the instantaneous calculation, weighted mean smoothing, and standard mean between windows, for the ADA and manual annotations. Outlier smoothing was evident near the 176 s and 189 s timestamps. The price for outlier smoothing was a slightly damped variability in the continuous heart rate measurement.

$$w_i = \frac{T_{N-i}}{\sum_i^N T_i} \tag{4}$$

Here w is the weight assigned to the HR value obtained in a particular window, T is the temporal length of the window, and N is the number of windows. The first window was assigned a weight based on the duration of the last window, and so on. The weight of a window was therefore inversely proportional to its duration. The final BTB evaluation was approximately equal to the BTB calculated for the smallest window (the instantaneous HR) albeit moderated by the larger windows (previous BTB values). The HR was then calculated as the inverse of the BTB measurement. The smoothing of the real-time HR measurement improved its readability.

2) Left Ventricular Ejection Time: The left ventricular ejection time (LVET) is a prominent CTI as it measures the delay between the aortic opening, t_{AO}, and closure, t_{AC}, during the systolic phase of the cardiac cycle,

$$LVET = t_{AC} - t_{AO} \tag{5}$$

The LVET indicates the amount of time taken for blood to leave the left ventricle, corresponding to an approximately 60% reduction in the volume of this chamber, measured as the left ventricular ejection fraction [56]. The morphological similarity in the AO-IC and AC-MO features necessitated a suppression of the AO-IC feature after identification, especially since it was typically stronger than the AC-MO feature.

The LVET was calculated using the same process as the extraction of BTB by amplification of the fiducial points in the SCG. First, the calculated heart rate was used to

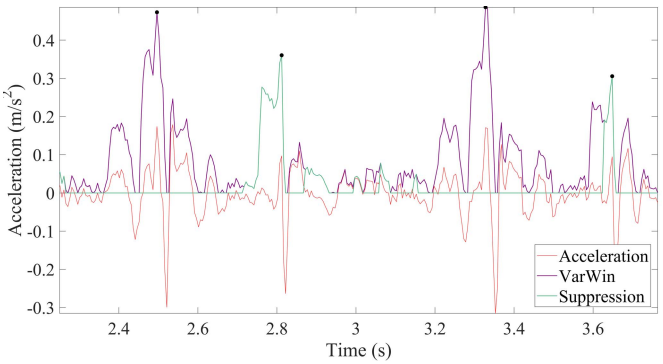

Fig. 7. Separation and identification of the AO and AC fiducial points in a 3 s window. The SCG (red) is processed to amplify the AO-IC drops (violet). Once identified, the region around the AO points is suppressed for identification of the AC-MO drops (green).

identify the AO points in the given window. The signal around each AO point and beyond each MO point was suppressed by nullifying the amplitude near local minima, as shown in Fig. 7. This suppression resulted in the AC-MO drop being the strongest feature in the SCG waveform, which was subsequently detected. The identification of the AC points allowed for a straightforward calculation of LVET using the previously determined AO points.

IV. Results

A. Analysis of Cardiac Activity

The ADA was tested on SCG signals obtained from subjects in the supine position that were measured twice when relaxed, and once when recovering from physical exertion, during a period of seven minutes for each measurement. DSP conducted on multiple window sizes produced a set of physiological measurements for each window, which were then averaged across windows using a weighted mean. The refresh rate was set to one second, implying that CRA was evaluated by the ADA at every one-second increment in measurement.

A set of ADA outputs for a subject with consistently high resting HRV are shown in Fig. 8 at rest (left) and during recovery (right). The SCG signal in Fig. 8.a was analyzed to deliver estimations of respiratory activity including:

1) respiration rate (RR) in Fig. 8.b,
2) respiration phase (classification of inhalation versus exhalation), estimated lung capacity, and inhalation volume relative to lung capacity in Fig. 8.c,

and measurements of cardiac activity including:

1) heart rate (HR) from ADA, manual annotation, and an upper-arm cuff sensor in Fig. 8.d,
2) beat-to-beat interval (BTB), left ventricular ejection time (LVET), and LVET as a fraction of BTB (LVETF) in Fig. 8.e.

The limitation that was imposed by setting the maximum window size to 10 s was evident in the respiration measurements. The minimum obtainable frequency component of the spectrum of the signal constrained within a 10 s window was 0.1 Hz, as compared to a normal, awake, resting RR of 0.2 Hz (12 breaths/minute). The subjects in this study generally had a relaxed respiration rate higher than this floor, but the measurement still appeared quantized as seen in Fig. 8.b due to the lack of resolution in the lower frequency side of the corresponding spectrum. In the frequency domain, considering the fact that the low frequency components relevant to orientation and motion artifact were already filtered, barely 3 to 5 accurate frequency points in the DFT were available over which to calculate respiratory activity. Hence the low resolution of the FFT within a small window size caused an apparent quantization of the relaxed respiration rate. In contrast, the recovery RR was less susceptible to this issue as the rate was typically high enough to obtain a more accurate calculation. The envelope of the Hilbert function for lung capacity calculation was also limited by the window size. Hence if the lungs did not inhale to their maximum capacity at least once during this time window, the estimated lung capacity decreased proportionately. This was evident in the lung capacity estimation for the recovery state in Fig. 8.c. Recovery and relaxed respiration rates also showed variation in their morphology, as the fraction of the respiratory cycle devoted to inhalation was lower for relaxed breathing. A comprehensive analysis of the effect of exertion on respiration would require acquisition outside a laboratory setting since a conscious awareness of breathing affects the respiratory cycle [57].

Heart rate variability as severe as 50 bpm was sometimes observed between beats during manual annotation of the SCG signals for recovering as well as relaxed subjects. The manually annotated heart-rate was processed using the same normalized weighted mean windowing as that used in the ADA. A sample result of this weighted smoothing feature was shown previously in Fig. 6. Heart rate measurement using the cuff was extracted at an indeterminable timestamp, because this measurement was taken during its deflation. As a result, the temporal error bars for the reference measurement in Fig. 8.d indicate the period of cuff deflation during which the measurement was known to have occurred. Vertical error bars correspond to a 95% accuracy of the measurement as per instrument specifications.

B. Verification of Hr Measurement Accuracy

The ADA was performed on each second of 12,958 seconds of data, including 18 seconds containing motion artifact. This corresponded to approximately 14,619 heartbeats that did not include motion artifact, as determined by a manual annotation of the AO peaks. Since the last of three measurement sets were conducted post-exercise, approximately a third of this data reflected measurements of recovery patterns immediately after physical exertion.

The accuracy of the ADA was benchmarked using the following two overlapping techniques: (i) by comparing the ADA measurements with manual annotations using the acquired experimental dataset, and (ii) by comparing the ADA measurements with ECG-based measurements using an external, publicly available dataset. The ADA was compared with manual annotations to quantify its beat detection accuracy in comparison to a trained eye. Regarding ECG, note that the reason SCG AO-AO intervals can be used as a surrogate for

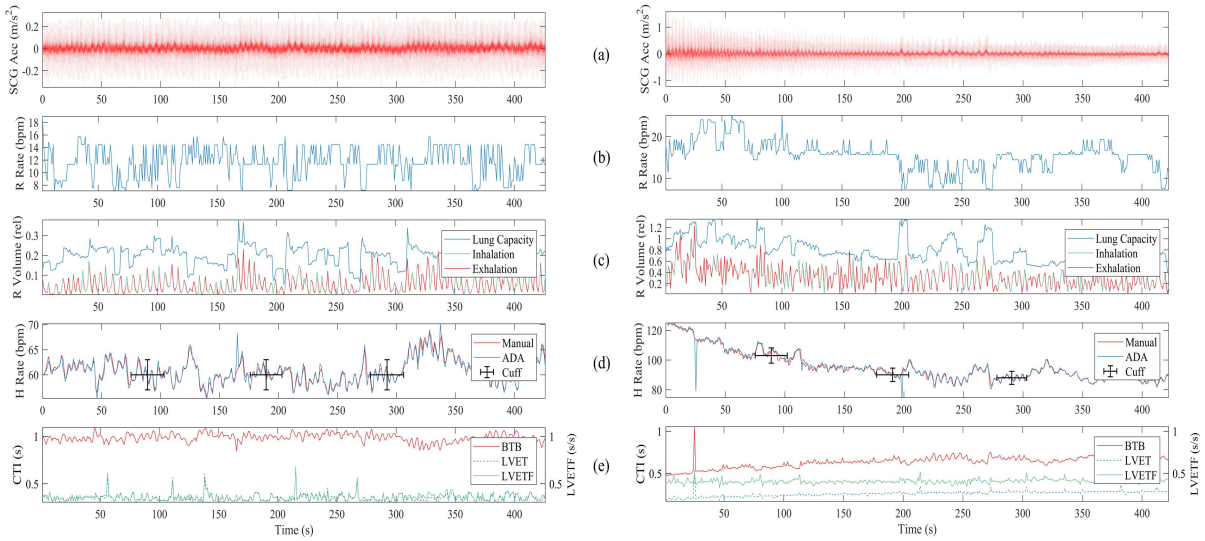

Fig. 8. (a) Vectorial magnitude of acceleration measured at the sternum over a 7-minute period for one supine subject when (left) relaxed and (right) recovering from physical exertion. The decline in cardiac and respiratory signal amplitudesduring recovery was noticeable, and is manifested in the results. (b) The respiration rate evaluation appeared more quantized for low-frequency values due to the lower resolution of the Fourier Transform given the limited window size. (c) The volume of air in the lungs was estimated from the oscillation amplitude of the most recent respiratory cycle. The angular phase of this oscillation determined the current respiration status as inhalation (green) or exhalation (red). The lung capacity estimation (blue) was based on the maximum inhalation volume of the largest window evaluated at each second. (d) Heart rate (blue) showed expectedly significant variability in the relaxed state, and was referenced with manual annotations (red) and a cuff sensor (black). (e) The decline in heart rate during recovery implied a rising beat-to-beat interval (red), and corresponded to a rising left ventricular ejection time (blue). Evidence of this can be seen in the relatively stable left ventricular ejection fraction (green).

ECG R-R intervals in traditional heart rate measurement is due to the strong agreement between the electrical R points and mechanical AO points. Hence as an unbiased quantification of accuracy, the ADA was further benchmarked using an externally sourced dataset consisting of ECG and SCG signals, on which it was not previously trained.

1) Accuracy Compared to Manual Annotations: Every SCG dataset was manually annotated to identify AO peaks and evaluate the corresponding BTB durations. The results were windowed to apply the same weighted mean smoothing as in the ADA evaluation of HR. Sections of the signal that were masked by noise were ignored during manual annotation, totaling 18 s worth of information in this study. The heart rate evaluation per second from both approaches was rounded to the nearest beat-per-minute value within two decimal places. Fig. 9 shows the correlation between HR measurements for each second of data, as well as the corresponding Bland-Altmann results. The 95% confidence intervals appear at less than ± 5 bpm, which is in agreement with the tolerance limits for the medical standard regarding heart-rate measurement [52].

A well-known drawback of the SCG acquisition method of CRA measurement is data corruption due to motion artifact such as movement, physical contact, or error from sensor misplacement. These issues mask the signal with noise and lead to measurement evaluation failures. In this test, the subjects remained motionless during acquisition, which provided a high signal-to-noise ratio for the detection of cardiac-induced vibrations as opposed to motion artifact. For certain situations, the ADA was able to account for a higher level of corrupted data in its evaluations than manual annotation. In most cases this provided a sensible estimate for heart rate despite masking of the AO points by noise or motion artifact, which rendered them manually unidentifiable. This was due to the flexibility of the ADA in identifying similarities between cardiac cycles in the rest of the signal around the AO instead of just the AO itself. Additionally, the feature amplification process of the VarWin function only identified relative changes with no consideration for absolute values or thresholding, which benefitted pattern recognition in the autocorrelation technique. The VarWin modified signal enabled a higher than expected accuracy for feature identification especially during periods of low signal quality of which the causes were speculated to be sensor misplacement, inhalation, or inadequate contact with the body. Another consequence of this approach was found to occur in the rare case where the AC-MO features caused a stronger differential acceleration than the AO-IC features. This pattern resulted in a stronger correlation at delays that corresponded to the duration between AC-AC beats instead of the expected AO-AO peaks. However, since the autocorrelation was blinded to the shapes of features in the signal, and since the MO peaks had a proportional delay from the AO peaks (due to low LVET variability as explained in Section IV-A combined with rapid AC-MO transition), the method still produced satisfactory results for HR albeit with outliers.

2) Accuracy Compared to Ecg on External Data: Manual annotations are susceptible to human error and observer bias. Such annotations do not conclusively prove the ability of the ADA to distinguish AO peaks from false positives such as motion artifacts that bear a similar resemblance to heartbeats (and would therefore also challenge the interpretation of the annotator). Therefore, as an additional test of reproducibility, the algorithm was used to analyze an external dataset consisting of synchronized Z-axis SCG, and ECG signals.

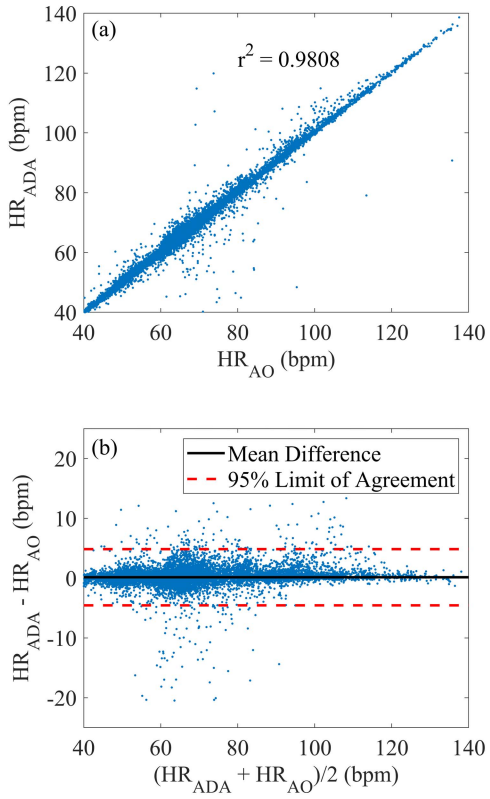

Fig. 9. (a) Scatter plot of ADA and manual SCG AO-AO heart rate fitted with a linear regression line with an r^2 correlation coefficient of 0.98. (b) Bland-Altman plot of heart rate computed from ADA and manual annotation with average error (black) and 95%-limits of agreement (red).

The data is available on the Physionet database [58], [59] and the algorithm was not designed for, or trained on, this externally sourced data. The data consisted of 17 subjects, with three sets of 200-second recordings, totaling 10,200 seconds across all subjects. The corresponding correlation and Bland-Altman plots are shown in Fig. 10. The test produced an r^2 of 0.8224 for HR measurements, which is expectedly lower than the accuracy correlation coefficient obtained by using the acquisition protocol in Section I.B for which the ADA was developed. The lower r^2 can therefore be attributed to possible variability in the positioning, acquisition method, noise, and motion artifact. The results validate the proposed approach by comparison with the ECG gold standard of HR measurement.

V. Discussion

As an extension of the work, a feasibility study was conducted on the algorithm to determine the following features: (i) robustness concerning AO detection during periods of high HRV, (ii) versatility of the ADA toward other SCG feature recognition such as AC detection and consequent LVET calculation, and (iii) algorithm efficiency constraints regarding speed and accuracy. In this context, the accuracy of AC detection was not determined. A comprehensive analysis including AC and LVET measurement would necessitate the acquisition of concurrent Impedance Cardiography (ICG) reference data and will be conducted in a future study. Finally, the efficiency characterization provided a useful tool to quantify the real-time capability of the algorithm.

A. Investigation of Ctis During Rest and Recovery

The LVET showed noticeably lower variability than BTB for relaxed measurements, indicating that the systolic phase of the cardiac cycle was relatively unaffected by HRV, as could be inferred from Fig. 11 with most of the temporal variability contained in the diastolic phase. The independence of LVET from relaxed BTB can be attributed to its origin: LVET is a result of the mechanical function of the heart, specifically the aortic valvular motion that acts in response to the dynamic pressure differential between the left ventricle and the aorta during the cardiac cycle. The occurrence of AO peaks on the other hand, are a consequence of the contraction of both ventricles triggered by the firing of the atrioventricular node, which relates to the pre-ejection period and corresponds to ECG measurements [9]. The evolution of the LVET in relation to the cardiac cycle can be seen in Fig. 8.e showing LVET, BTB, and the duration of the LVET as a fraction (LVETF) of the BTB duration,

$$LVETF = \frac{LVET}{BTB} \tag{6}$$

The LVETF was less responsive to changes in HR as can be seen during post-exercise recovery. An improved stability at higher heart rates was attributed to lower HRV [60]. As a consequence of this relationship between LVET and BTB, the LVET is typically corrected using the HR as determined by a metric called the left ventricular ejection time index (LVETI) accurate up to 150 bpm [61], and given by [62],

$$LVETI = LVET + 0.0017 \times HR \tag{7}$$

The characterization of exertion is relatively difficult in SCG due to an implicit and proportional increase in motion artifact. This offers limited depth for studies on SCG morphology performed during exertion, and requires referencing with ECG [63]. Our protocol worked around the problem by measuring supine subjects immediately after undergoing intense exertion, that is, during post-exercise recovery. The validity of this approach is demonstrated in Fig. 11 which visualizes the result of averaging relaxed and exerted cardiac cycles over 300 heart beats, when lined up at their respective AO fiducial points. For the relaxed state in Fig. 11.a, a sharp AC-MO coincidence was seen between the waveforms despite the cycles being different lengths due to HRV, whereas normalizing the cycle durations (to a period of 1 s each in Fig. 11.b) induced an AC-MO mismatch. In the recovery state however, while following cardiac activity from exertion (violet) to relaxation (red) in Fig. 11.c, the decreasing BTB blurred any AC-MO overlap between multiple waveforms, and this became apparent when considering the clear AC-MO overlap that was obtained in Fig. 11.d after temporally normalizing the waveforms to a 1 s duration.

It is worth noting that the amplitude of AO acceleration also showed a consistent decline during recovery. This is in contrast to the acceleration of the AC-MO variation that instead consistently increased in amplitude and therefore definition, as heart rate returned to a normal resting state.

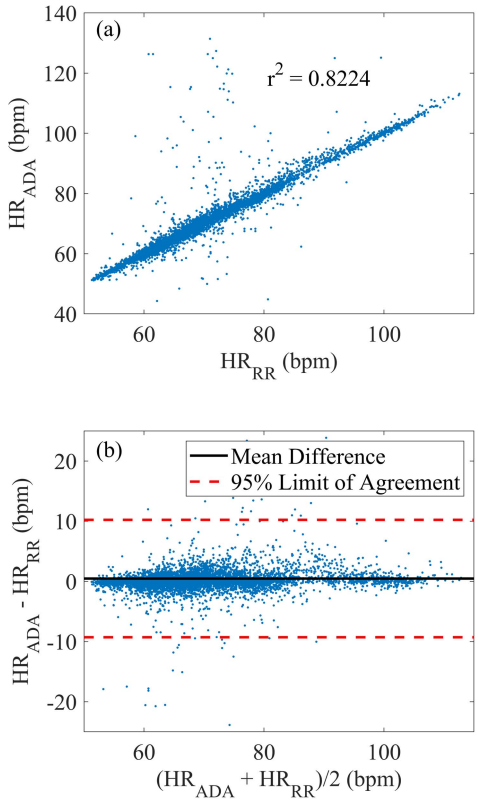

Fig. 10. (a) Scatter plot of ADA AO-AO and ECG R-R heart rate calculations fitted with a linear regression line with an r^2 correlation coefficient of 0.8224. (b) Bland-Altman plot of heart rate computed from ADA and ECG with average error (black) and 95%-limits of agreement (red).

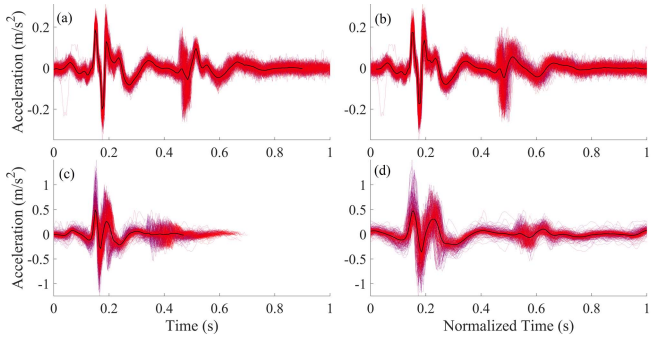

Fig. 11. Time-averaged SCG waveforms for 300 heartbeats in the relaxed (top) and post-exercise recovery (bottom) states for raw (left) and temporally normalized (right) cardiac cycles. HRV in relaxed SCG did not propagate into LVET as can be seen from the clarity of the signal in (a), and the blurring of the signal when the cardiac cycles were temporally normalized (scaled to a duration of one second) in (b). However, HRV is less prominent for exerted SCG (c), which facilitated accurate detection of LVET by temporally normalizing the signal (d). This helped account for weaker detection as a consequence of the suppression of the AC-MO feature with increasing exertion.

These results were consistent with cardiological studies relating a decline in HRV with exertion, as well as a decline in systolic time intervals (STIs) [64]. The LVETI was calculated as an indication of STI trends, as it is more strongly influenced by HR than the pre-ejection period [65]. Consequently, the LVETI and HRV were evaluated at 1s intervals (as explained in Section IV-A) within the ADA framework,

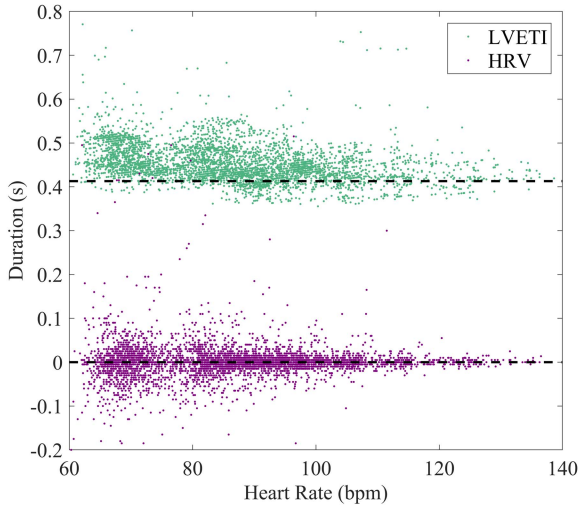

Fig. 12. LVETI and HRV calculated using LVET and BTB values from the smallest viable window of each measurement. The values are taken from exclusively the recovery datasets of all 10 subjects. LVETI (green) was calculated as in equation (7) for healthy males, and HRV (violet) was calculated as the successive differences between beats represented by the AO points. Expected mean values are represented as dashed black lines.

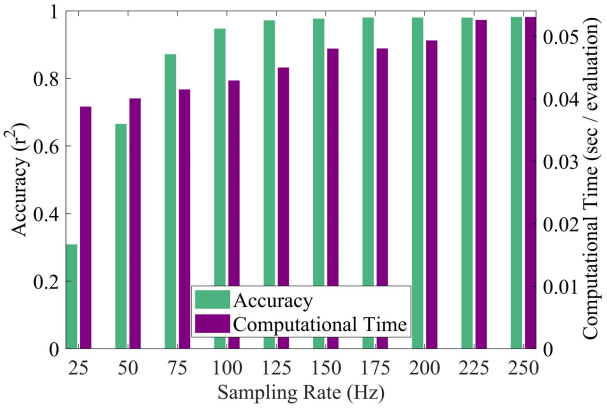

Fig. 13. Characterization of the ADA performance for accuracy and computational time. The computational time was evaluated as the runtime in seconds required for each evaluation of all output physiological metrics. It therefore indicates the upper limit of the ADA refresh rate. The clock supplied by the operating system for performance measurement through the MATLAB profiler was used for this purpose. Accuracy was measured as the correlation coefficient between HR produced by the ADA, and by manual AO annotation.

and are depicted in Fig. 12 for the recovery datasets of all 10 subjects. The root mean square of successive differences (RMSSD) and standard deviation (SD) are commonly used metrics of HRV [66]. When calculated from the AO points, both metrics showed an inverse relationship with heart rate, as depicted by the convergence of values towards the right in Fig. 12. As the level of exertion increased, the HR rose, and the variability in BTB declined. Interestingly, the HRV was found to reduce significantly despite the fact that the BTB was already continuously increasing as the subject naturally recovered. Despite the fact that the recovery trajectory of the subject had not been calibrated out of this depiction, the HRV still clearly reduced with HR. Additionally, evaluations of LVETI during exertion appeared to be constrained to a

minimum value as shown in the form of a dashed black line. The linear regression equation for LVETI intersected with the median LVETI of 0.446 s at a heart rate of 94 bpm, which was approximately equal to the median of measured heart rates, and therefore suggested a uniform distribution. The distribution was in general agreement with the expected LVETI of 0.413 s (dashed black line) for healthy males with allowance for daily fluctuations, outliers, and variability [67], but also suggests that the algorithm has potential for improvement.

The relationship between HRV and systolic time intervals such as LVET, particularly within the context of physical stress, offers insights into cardiac performance, autonomic regulation, and possible disease prediction based on the reactivity hypothesis [68]. Longer measurement periods with larger populations and standard referencing will be required to evaluate the ability of the ADA to quantify exertion from CRA. These measurements highlight the potential of the ADA code for deeper analyses of cardiac-induced sternal vibrations, which will be explored in future studies.

B. Performance: Computational Time

The ADA approach was characterized for algorithm performance at different sampling frequencies. The lowest acceptable frequency retaining basic SCG morphology was found to be 50 Hz with $r^2 > 0.5$. Previous investigations have detected the occurrence of cardiac events such as valvular activity and murmurs that contain frequency components as high as 320 Hz [69]. Current state of the art algorithms typically sample above 200 Hz [29], [31], [34]. However, we have found that the ADA accuracy did not significantly improve beyond 150 Hz. Admittedly, the accuracy was quantified for only heart rate measurements and no other features in SCG morphology such as LVET. For further analysis of SCG morphology, a higher sampling rate may be required.

The performance was measured on a 2.6 GHz Intel i7-770HQ processor with 16 GB 2133 MHz LPDDR3 memory. The performance of the algorithm was evaluated at different sampling frequencies using accuracy (correlation coefficient) and computational time as characterization metrics, as shown in Fig. 13. An intuitive observation is the trade-off between accuracy and computational requirement for different sampling frequencies. The ADA computational time was linearly dependent on sampling frequency, which contrasts other algorithms available in the literature whose computational time have been found to increase exponentially with sampling frequency. An optimal operational efficiency was seen at a sampling frequency of 100 Hz, although acceptable accuracy or computational time was obtained at 75 Hz or 125 Hz respectively, as well. Recommended operating frequency is 200 Hz as this allows real-time measurements requiring 0.05 s runtime for each second of measurement data, with an accuracy close to the maximum, and well within medical standards [52]. The metrics of computational time and accuracy in Fig. 13 represent, to our knowledge, the only efficiency characterization over sampling frequency that has been reported in the literature for a real-time SCG detection algorithm.

C. Extensions

The ADA autocorrelation-based technique provided a customized pattern recognition tool to amplify relevant SCG features for analysis. The functionality was supported by a combination of first principles (e.g., the VarWin) and statistical methods (e.g., autocorrelation for feature detection). This provides a useful framework for future integration with learning algorithms, deeper analyses of cardiac time intervals such as LVET, and feature recognition and identification to determine cardiac behavior. Due to the large variability in SCG morphology and the need to adapt to large amounts of data without standardized waveforms, machine learning techniques would be useful to develop future SCG algorithms. The combined approach would allow for further refinement using regression or classification algorithms to improve, for example, heart rate calculations, motion artifact filtration, and beat identification. Currently, however, it is our belief that the ADA still has scope for improvement using further fundamental modeling of cardiac-induced vibrational wave propagation through the chest, and the relation to SCG morphology and variability. Supervised learning algorithms trained on the raw data could also improve tasks such as detection accuracy and motion artifact filtration, which would significantly benefit from rigorous statistical approaches.

VI. Conclusion

The ADA represents a novel approach for the non-invasive and real-time measurement of specific physiological activity. It was applied to the extraction of CRA measurements from accelerometer data. Data was collected from ten subjects in the supine position for three 7-minute-long sets. This represented measurements over 14,619 heartbeats within 12,958 seconds. Respiratory activity was also evaluated from the SCG signals. Temporal windowing and autocorrelation-based pattern recognition were employed to detect and amplify characteristic features in the SCG signal, whilst accounting for variations and noise from issues such as motion artifact or sensor misplacement. Fiducial points of interest were used to determine time intervals within, and between, consecutive cardiac cycles.

For the prediction of heart rate, the accuracy was compared with a medical reference device and manual verification on all data sets. The computational efficiency of this approach was found to be significantly high as compared to algorithms available in the literature. This suggests easy scalability to a variety of platforms for a real-time, reliable evaluation of physiological measurements. However, increasing the sampling frequency showed diminishing returns in accuracy beyond 125 Hz, which indicated a possible Nyquist limit for SCG features relevant to the ADA.

We have therefore demonstrated the performance of an algorithm capable of providing CRA-relevant metrics in real-time. Considering the heart rate of a supine subject, the accuracy was within the standards for a medical device. An acquisition rate as low as 100 Hz still delivered heart rate accuracy within medical standards [52] and therefore allows for options for lower power energy consumption when implemented in a portable system. The algorithm also demonstrated basic

motion artifact cancellation in its evaluation of physiological metrics.

ACKNOWLEDGMENT

Y. D'Mello and D. Plant would like to acknowledge the NSERC Canada Graduate Scholarships and NSERC CREATE Silicon Electronic-Photonic Integrated Circuits (SiEPIC) programs for scholarship funding and access to educational material. Experimental work and development of the ADA was performed at McGill University and MacDonald, Dettwiler and Associates Corporation. Software and physical resources were obtained with support from the Canadian Microelectronics Corporation (CMC) and McGill University.

REFERENCES

[1] E. Benjamin *et al.*, "Heart disease and stroke statistics-2018 update: A report from the american heart association," *Circulation*, vol. 137, no. 12, pp. e67–e492, 2018.

[2] A. Cohen *et al.*, "Estimates and 25-year trends of the global burden of disease attributable to ambient air pollution: An analysis of data from the global burden of diseases study 2015," *Lancet*, vol. 389, no. 10082, pp. 1907–1918, 2017.

[3] J. Y. A. Foo and S. J. Wilson, "A computational system to optimise noise rejection in photoplethysmography signals during motion or poor perfusion states," *Med. Biol. Eng. Comput.*, vol. 44, nos. 1–2, pp. 140–145, 2006.

[4] O. T. Inan *et al.*, "Ballistocardiography and seismocardiography: A review of recent advances," *IEEE J. Biomed. Health Inform.*, vol. 19, no. 4, pp. 1414–1427, Jul. 2015.

[5] J. Topouchian *et al.*, "Validation of four automatic devices for self-measurement of blood pressure according to the international protocol of the European society of hypertension," *Vascular Health Risk Manage.*, vol. 7, no. 4, pp. 709–717, 2011.

[6] K. Tavakolian, "Systolic time intervals and new measurement methods," *Cardiovascular Eng. Technol.*, vol. 7, no. 2, pp. 118–125, 2016.

[7] B. S. Bozhenko, "Seismocardiography-a new method in the study of functional conditions of the heart [in Russian]," *Terapevticheskii arkhiv*, vol. 33, pp. 55–64, Sep. 1961.

[8] R. M. Baevskii, A. D. Egorov, and L. A. Kazarian, "The method of seismocardiography," *Kardiologiia*, vol. 18, pp. 87–89, 1964.

[9] J. M. Zanetti and D. M. Salerno, "Seismocardiography: A technique for recording precordial acceleration," in *Proc. Comput.-Based Med. Syst. 4th Annu. IEEE Symp.*, May 1991, pp. 4–9.

[10] K. Pandia, O. T. Inan, G. T. A. Kovacs, and L. Giovangrandi, "Extracting respiratory information from seismocardiogram signals acquired on the chest using a miniature accelerometer," *Physiol. Meas.*, vol. 33, no. 10, pp. 1643–1660, 2012.

[11] N. Alamdari, K. Tavakolian, V. Zakeri, R. Fazel-Rezai, and A. Akhbardeh, "A morphological approach to detect respiratory phases of seismocardiogram," in *Proc. 38th Annu. Int. Conf. IEEE Eng. Med. Biol. Soc. (EMBC)*, Aug. 2016, pp. 4272–4275.

[12] V. Zakeri, A. Akhbardeh, N. Alamdari, R. Fazel-Rezai, M. Paukkunen, and K. Tavakolian, "Analyzing seismocardiogram cycles to identify the respiratory phases," *IEEE Trans. Biomed. Eng.*, vol. 64, no. 8, pp. 1786–1792, Aug. 2017.

[13] M. J. Tadi, T. Koivisto, and M. Pänkäälä, "Accelerometer-based method for extracting respiratory and cardiac gating information for dual gating during nuclear medicine imaging," *Int. J. Biomed. Imag.*, vol. 2014, Jul. 2014, Art. no. 690124.

[14] B. Aysin and E. Aysin, "Effect of respiration in heart rate variability (HRV) analysis," in *Proc. Int. Conf. IEEE Eng. Med. Biol. Soc.*, Aug./Sep. 2006, pp. 1776–1779.

[15] Y. Fang, J.-T. Sun, C. Li, C.-S. Poon, and G.-Q. Wu, "Effect of different breathing patterns on nonlinearity of heart rate variability," in *Proc. 30th Annu. Int. Conf. IEEE Eng. Med. Biol. Soc.*, Aug. 2008, pp. 3220–3223.

[16] T. Buchner, "HRV strongly depends on breathing. Are we questioning the right suspect?" in *Proc. Annu. Int. Conf. IEEE Eng. Med. Biol. Soc.*, Aug./Sep. 2011, pp. 7739–7742.

[17] N. Davidson, S. Goldner, and D. I. McCloskey, "Respiratory modulation of barareceptor and chemoreceptor reflexes affecting heart rate and cardiac vagal efferent nerve activity," *J. Physiol.*, vol. 259, no. 2, pp. 523–530, 1976.

[18] M. A. Cretikos, R. Bellomo, K. Hillman, J. Chen, S. Finfer, and A. Flabouris, "Respiratory rate: The neglected vital sign," *Proc. MJA*, vol. 188, no. 11, pp. 657–659, 2008.

[19] R. Crow, P. Hannan, D. Jacobs, L. Hedquist, and D. M. Salerno, "Relationship between seismocardiogram and echocardiogram for events in the cardiac cycle," *Amer. J. Noninvasive Cardiol.*, vol. 8, no. 1, pp. 39–46, 1994.

[20] M. D. Rienzo *et al.*, "Wearable seismocardiography: Towards a beat-by-beat assessment of cardiac mechanics in ambulant subjects," *Autonomic Neurosci.*, vol. 178, nos. 1–2, pp. 50–59, 2013.

[21] M. Etemadi, O. T. Inan, J. A. Heller, S. Hersek, L. Klein, and S. Roy, "A wearable patch to enable long-term monitoring of environmental, activity and hemodynamics variables," *IEEE Trans. Biomed. Circuits Syst.*, vol. 10, no. 2, pp. 280–288, Apr. 2016.

[22] P. K. Sahoo, H. K. Thakkar, and M.-Y. Lee, "A cardiac early warning system with multi channel SCG and ECG monitoring for mobile health," *Sensors*, vol. 17, no. 4, p. 711, 2017.

[23] J. M. Zanetti and K. Tavakolian, "Seismocardiography: Past, present and future," in *Proc. 35th Annu. Int. Conf. IEEE Eng. Med. Biol. Soc. (EMBC)*, Jul. 2013, pp. 7004–7007.

[24] D. M. Salerno and J. Zanetti, "Seismocardiography for monitoring changes in left ventricular function during ischemia," *Chest*, vol. 100, no. 4, pp. 991–993, 1991.

[25] M. Becker *et al.*, "Simplied Detection Of Myocardial Ischemia by Seismocardiography," *Herz*, vol. 39, 2014.

[26] K. Tavakolian, G. A. Dumont, G. Houlton, and A. P. Blaber, "Precordial vibrations provide noninvasive detection of early-stage hemorrhage," *Shock*, vol. 41, no. 2, pp. 91–96, 2014.

[27] A. Sundar and V. Pahwa, "Evaluating the performance of state of the art algorithms for enhancement of seismocardiogram signals," in *Proc. 1st Int. Conf. Intell. Comput.*, 2016, pp. 37–45.

[28] F. Khosrow-Khavar, K. Tavakolian, A. Blaber, and C. Menon, "Automatic and robust delineation of the fiducial points of the seismocardiogram signal for noninvasive estimation of cardiac time intervals," *IEEE Trans. Biomed. Eng.*, vol. 64, no. 8, pp. 1701–1710, Aug. 2017.

[29] J. Wahlström *et al.*, "A hidden markov model for seismocardiography," *IEEE Trans. Biomed. Eng.*, vol. 64, no. 10, pp. 2361–2372, Oct. 2017.

[30] A. Laurin, F. Khosrow-Khavar, A. P. Blaber, and K. Tavakolian, "Accurate and consistent automatic seismocardiogram annotation without concurrent ECG," *Physiol. Meas.*, vol. 37, no. 9, pp. 1588–1604, 2016.

[31] M. D. Rienzo, E. Vaini, and P. Lombardi, "An algorithm for the beat-to-beat assessment of cardiac mechanics during sleep on Earth and in microgravity from the seismocardiogram," *Sci. Rep.*, vol. 7, no. 1, 2017, Art. no. 15634.

[32] M. Malcangi, H. Quan, E. Vaini, P. Lombardi, and M. D. Rienzo, "Applying the EFuNN evolving paradigm to the recognition of artefactual beats in continuous seismocardiogram recordings," in *Proc. Int. Conf. Eng. Appl. Neural Netw.*, 2017, pp. 256–264.

[33] F. Khosrow-Khavar, K. Tavakolian, A. P. Blaber, J. M. Zanetti, R. Fazel-Rezai, and C. Menon, "Automatic annotation of seismocardiogram with high-frequency precordial accelerations," *IEEE J. Biomed. Health Inform.*, vol. 19, no. 4, pp. 1428–1434, Jul. 2015.

[34] M. J. Tadi *et al.*, "A real-time approach for heart rate monitoring using a hilbert transform in seismocardiograms," *Physiol. Meas.*, vol. 37, no. 11, pp. 1885–1909, 2016.

[35] C. A. Wick, O. T. Inan, J. H. McClellan, and S. Tridandapani, "Seismocardiography-based detection of cardiac quiescence," *IEEE Trans. Biomed. Eng.*, vol. 62, no. 8, pp. 2025–2032, Aug. 2015.

[36] J. W. Dukes *et al.*, "Ventricular ectopy as a predictor of heart failure and death," *J. Amer. College Cardiol.*, vol. 66, no. 2, pp. 101–109, 2015.

[37] J. Thayer, S. S. Yamamoto, and J. F.Brosschot, "The relationship of autonomic imbalance, heart rate variability and cardiovascular disease risk factors," *Int. J. Cardiol.*, vol. 141, no. 2, pp. 122–131, 2010.

[38] C. Guilleminault, S. J. Connolly, and R. A. Winkle, "Cardiac arrhythmia and conduction disturbances during sleep in 400 patients with sleep apnea syndrome," *Amer. J. Cardiol.*, vol. 52, no. 5, pp. 490–494, 1983.

[39] A. Laurin, "New timing estimations of cardiovascular events; applications to seismocardiography, microneurography, and blood pressure," Ph.D. dissertation, Dept. Biomed. Physiol. Kinesiology, Simon Fraser Univ., Burnaby, BC, Canada, 2015.

[40] H. Ashouri and O. T. Inan, "Automatic detection of seismocardiogram sensor misplacement for robust pre-ejection period estimation in unsupervised settings," *IEEE Sensors J.*, vol. 17, no. 12, pp. 3805–3813, Jun. 2017.

[41] G. Shafiq, S. Tatinati, and K. C. Veluvolu, "Automatic annotation of peaks in seismocardiogram for systolic time intervals," in *Proc. 38th Annu. Int. Conf. IEEE Eng. Med. Biol. Soc. (EMBC)*, Aug. 2016, pp. 2672–2675.
[42] K. Tavakolian *et al.*, "Precordial acceleration signals improve the performance of diastolic timed vibrations," *Med. Eng. Phys.*, vol. 35, no. 8, pp. 1133–1140, 2013.
[43] P. Reant *et al.*, "Systolic time intervals as simple echocardiographic parameters of left ventricular systolic performance: Correlation with ejection fraction and longitudinal two-dimensional strain," *Eur. J. Echocardiography*, vol. 11, no. 10, pp. 834–844, 2010.
[44] J. Ärnlöv, E. Ingelsson, U. Risérus, B. Andrén, and L. Lind, "Myocardial performance index, a doppler-derived index of global left ventricular function, predicts congestive heart failure in elderly men," *Eur. Heart J.*, vol. 25, no. 24, pp. 2220–2225, 2004.
[45] J. A. Hirsch and B. Bishop, "Respiratory sinus arrhythmia in humans: How breathing pattern modulates heart rate," *Amer. J. Physiol.-Heart Circulatory Physiol.*, vol. 241, no. 4, pp. H620–H629, 1981.
[46] J. Turner, "Maximal exercise stress test," in *Encyclopedia of Behavioral Medicine*. New York, NY, USA: Springer, 2013.
[47] C. Brüser, S. Winter, and S. Leonhardt, "Robust inter-beat interval estimation in cardiac vibration signals," *Physiol. Meas.*, vol. 34, no. 2, p. 123, 2013.
[48] O. Lahdenoja, T. Humanen, M. J. Tadi, M. Pänkäälä, and T. Koivisto, "Heart rate variability estimation with joint accelerometer and gyroscope sensing," in *Proc. Comput. Cardiol. Conf. (CinC)*, Sep. 2016, pp. 717–720.
[49] A. M. Weissler, W. S. Harris, and C. D. Schoenfeld, "Systolic time intervals in heart failure in man," *Circulation*, vol. 37, no. 2, pp. 149–159, 1968.
[50] T. Hurnanen *et al.*, "Automated detection of atrial fibrillation based on time-frequency analysis of seismocardiograms," *IEEE J. Biomed. Health Inform.*, vol. 21, no. 5, pp. 1233–1241, Sep. 2017.
[51] P. Van Leeuwen and H. C. Kuemmell, "Respiratory modulation of cardiac time intervals," *Heart*, vol. 58, no. 2, pp. 129–135, 1987.
[52] "Cardiac monitors, heart rate meters, and alarms," Assoc. Adv. Med. Instrum. Arlington, VA, USA, Tech. Rep. ANSI/AAMI EC13, 2002.
[53] C. P. Subbe, M. Kruger, P. Rutherford, and L. Gemmel, "Validation of a modified early warning score in medical admissions," *QJM Int. J. Med.*, vol. 94, no. 10, pp. 521–526, 2001.
[54] M. D. Charles, D. Cook, B. A. Joanna, and F. Hamann, "Relation of lung volumes to height in healthy persons between the ages of 5 and 38 years," *J. Pediatrics*, vol. 59, no. 5, pp. 710–714, 1961.
[55] R. Q. Migrino, R. K. Mareedu, D. Eastwood, M. Bowers, L. Harmann, and P. Hari, "Left ventricular ejection time on echocardiography predicts long-term mortality in light chain amyloidosis," *J. Amer. Soc. Echocardiography*, vol. 22, no. 12, pp. 1396–1402, 2009.
[56] H. T. Dodge, H. Sandler, W. A. Baxley, and R. R. Hawley, "Usefulness and limitations of radiographic methods for determining left ventricular volume," *Amer. J. Cardiol.*, vol. 18, no. 1, pp. 10–24, 1966.
[57] R. Gilbert, J. H. Auchincloss, Jr., J. Brodsky, and W Boden, "Changes in tidal volume, frequency, and ventilation induced by their measurement," *J. Appl. Physiol.*, vol. 33, no. 2, pp. 252–254, 1972.
[58] M. A. García-González, A. Argelagós-Palau, M. Fernández-Chimeno, and J. Ramos-Castro, "A comparison of heartbeat detectors for the seismocardiogram," in *Proc. Comput. Cardiol.*, vol. 40, Sep. 2013, pp. 461–464.
[59] A. L. Goldberger *et al.*, "PhysioBank, PhysioToolkit, and PhysioNet: Components of a new research resource for complex physiologic signals," *Circulation*, vol. 101, no. 23, pp. e215–e220, 2000.
[60] M. Javorka *et al.*, "Heart rate recovery after exercise: Relations to heart rate variability and complexity," *Brazilian J. Med. Biol. Res.*, vol. 35, no. 8, pp. 991–1000, 2002.
[61] A. Weissler, L. C. Harris, and G. D. White, "Left ventricular ejection time index in man," *J. Appl. Physiol.*, vol. 18, no. 5, pp. 919–923, 1963.
[62] A. M. Weissler, W. S. Harris, and C. D. Schoenfeld, "Systolic time intervals in heart failure in man," *Circulation.*, vol. 37, no. 2, pp. 149–159, 1968.
[63] M. D. Rienzo, E. Vaini, P. Castiglioni, P. Meriggi, and F. Rizzo, "Beat-to-beat estimation of LVET and QS2 indices of cardiac mechanics from wearable seismocardiography in ambulant subjects," in *Proc. 35th Annu. Int. Conf. IEEE Eng. Med. Biol. Soc. (EMBC)*, Jul. 2013, pp. 7017–7020.
[64] S. Michael, K. S. Graham, and G. M. Davis, "Cardiac autonomic responses during exercise and post-exercise recovery using heart rate variability and systolic time intervals—A review," *Frontiers Physiol.*, vol. 8, p. 301, May 2017.
[65] C. L. Garrard Jr., M. Arnold, and M. Weissler, and H. T. Dodge, "The relationship of alterations in systolic time intervals to ejection fraction in patients with cardiac disease," *Circulation*, vol. 42, no. 3, pp. 455–462, 1970.
[66] F. Shaffer and J. P. Ginsberg, "An overview of heart rate variability metrics and norms," *Frontiers Public Health*, vol. 5, p. 258, Sep. 2017.
[67] R. P. Lewis, S. E. Rittogers, W. F. Froester, and H. Boudoulas, "A critical review of the systolic time intervals," *Circulation*, vol. 56, no. 2, pp. 146–158, 1977.
[68] D. S. Krantz and S. B. Manuck, "Acute psychophysiologic reactivity and risk of cardiovascular disease: A review and methodologic critique," *Psychol. Bull.*, vol. 96, no. 3, pp. 435–464, 1984.
[69] K. Tavakolian, "Characterization and analysis of seismocardiogram for estimation of hemodynamic parameters," Ph.D. dissertation, School Eng. Sci., Simon Fraser Univ., Burnaby, BC, Canada, 2010.

Yannick D'Mello received the B.Eng. degree in engineering physics with a minor in economics from Carleton University, Ottawa, in 2015. He is currently pursuing the Ph.D. degree in dynamic energy-matter interactions with McGill University. His research interests include acoustic, photonic, electronic, and magnetic wave propagation and interference; emitters, modulators, and absorbers; signal processing; sensors and actuators; and smart, crystalline, and meta materials.

James Skoric received the B.Eng. degree in electrical engineering from McGill University, Montreal, QC, Canada, in 2018, where he is currently pursuing the M.Eng. degree. His research interests include wearable sensors, physiological monitoring, and biosignal processing.

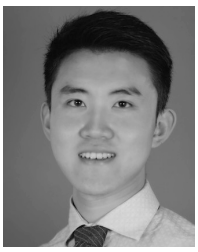

Shicheng Xu received the B.Eng. degree in electrical engineering from McGill University, Montreal, Canada, in 2018. He is currently pursuing the M.S.E. degree in biomedical engineering with Johns Hopkins University, Baltimore, MD, USA. His main research interest includes the design of wearable medical devices.

Megan Akhras received the B.Eng. degree from McGill University in 2018 with a major in Electrical Engineering and a minor in Biomedical Engineering. During her years at McGill University, she led a team of electrical engineering students in McGill robotics. She also worked on systems integration with Zimmer Biomet and IT Advisory for Financial Services at EY. She is currently with Accenture as a part of Technology services.

Philip J. R. Roche received the Ph.D. degree from the University of Manchester (CEAS, Manchester, U.K.) in 2008, where he is currently a Biotechnology Consultant.

Michel A. Lortie received the degree in mechanical engineering from the University of Ottawa, where he has been a computer and systems designer for over 40 years. He is currently a Professional Engineer registered in Ontario and Québec. His design activities have led to implementations in all segments of a modern industrial economy, including manufacturing, process control, aerospace, pharmaceutical, and healthcare industries. His current research interests include clinical decision support systems and cognitive workload assessment.

Stéphane Gagnon received the bachelor's degree in electrical engineering from the École Polytechnique de Montréal and the master's degree in business administration from the University of Ottawa. He has over 20 years' experience in project management and the development of complex electrical systems for aerospace, telecommunication, military, and medical applications. He held various positions at Neptec Design Group, where he is currently the Vice President of Space Programs.

David V. Plant (F'07) received the Ph.D. degree from Brown University, Providence, RI, USA, in 1989. He was a Research Engineer with the University of California Los Angeles, Los Angeles, CA, USA, from 1989 to 1993. He has been a Professor with McGill University, Montreal, QC, Canada, since 1993, where he holds the James McGill Professorship. He has published more than 400 journal and conference papers and has one licensed patent. He has received five teaching awards and numerous other awards, including the IEEE Photonics Society Distinguished Lectureship and the IEEE Microwave Theory and Techniques Society Microwave Prize. He is a Fellow of OSA, the Engineering Institute of Canada, and the Canadian Academy of Engineering. He currently holds a Killam Research Fellowship.